

# HH 175: A Giant HH Flow Emanating From A Multiple Protostar

Bo Reipurth<sup>1\*</sup> and Per Friberg<sup>2</sup>

<sup>1</sup> *Institute for Astronomy, University of Hawaii at Manoa, 640 N. Aohoku Place, Hilo, HI 96720, USA*

<sup>2</sup> *James Clark Maxwell Telescope, East-Asian Observatory, 660 North Aohoku Place, Hilo, HI 96720, USA*

Accepted XXX. Received YYY; in original form ZZZ

## ABSTRACT

HH 175 is an isolated Herbig-Haro object seen towards the B35 cloud in the  $\lambda$  Ori region. We use deep Subaru 8m interference filter images and Spitzer images to show that HH 175 is a terminal shock in a large collimated outflow from the nearby embedded source IRAS 05417+0907. The body of the eastern outflow lobe is hidden by a dense ridge of gas. The western outflow breaks out of the front of the cometary-shaped B35 cloud, carrying cloud fragments along, which are optically visible due to photoionization by the massive  $\lambda$  Ori stars. The total extent of the bipolar outflow is 13.7 arcmin, which at the adopted distance of 415 pc corresponds to a projected dimension of 1.65 pc. The embedded source IRAS 05417+0907 is located on the flow axis approximately midway between the two lobes, and near-infrared images show it to be a multiple system of 6 sources, with a total luminosity of 31  $L_{\odot}$ . Millimeter maps in CO,  $^{13}\text{CO}$ , and  $\text{C}^{18}\text{O}$  show that the B35 cloud is highly structured with multiple cores, of which the one that spawned IRAS 05417+0907 is located at the apex of B35. It is likely that the embedded source is the result of compression by an ionization-shock front driven by the  $\lambda$  Ori OB stars.

**Key words:** Herbig-Haro objects — ISM: jets and outflows — shocks — stars: formation — stars: protostars — stars: pre-main sequence

## 1 INTRODUCTION

In the mid- to late 1990’s, with the advent of large-format CCDs, it was recognized that Herbig-Haro (HH) objects can be part of giant shocked outflow structures extending on a scale of one to several parsec (e.g., Reipurth et al. 1997a). Of the more than 1000 HH flows known, several dozen have been identified as having parsec-scale dimensions. For reviews on HH objects, see Reipurth & Bally 2001, Bally 2016). We here present the discovery and study of a new giant HH flow located in the Barnard 35 (B35) cloud in the  $\lambda$  Ori star forming region.

$\lambda$  Orionis is an O8III star (Conti & Leep 1974) that is part of a small group of OB stars (Murdin & Penston 1977) which excites the HII region Sh2-264 (Sharpless 1959, Sahana & Haffner 2016). Bordering and bounding the HII region (which has an electron density of about  $2\text{ cm}^{-3}$  and a mass of about  $5 \times 10^3 M_{\odot}$ ) is a large ring or shell of molecular clouds, detected in the optical and in neutral hydrogen (Wade 1957; Heiles & Habing 1974, Sahana & Haffner 2016), in molecular gas (Maddalena et al. 1986, Maddalena and Morris 1987), and at mid- and far-infrared wavelengths (Zhang et al. 1989). The shell is highly structured, with the most massive part in the north-west section. The mass of HI in the ring has been estimated to be about  $4.5 \times 10^4 M_{\odot}$  (Wade 1957). Maddalena & Morris (1987) adopt a value of about  $1 \times 10^4 M_{\odot}$  for HI and about  $3 \times 10^4 M_{\odot}$  for  $\text{H}_2$  associated with the remaining molecular clouds. Thus the total mass of gas in the ring is about  $4 \times 10^4 M_{\odot}$  (this number has at least a factor of 2 uncertainty). The original molecular cloud that gave birth to this small OB association must have had a mass of order  $5 \times 10^4 M_{\odot}$ ,

typical for a small GMC. The dynamical age of the expanding ring is about  $5 \times 10^6$  years, in agreement with estimates of the age of the  $\lambda$ -Ori OB sub-group.

$\lambda$  Ori is the most massive member of a loose cluster, Collinder 69, which contains several hundred young low-mass stars, detected by their  $\text{H}\alpha$  emission (Joy 1949, Haro et al. 1953, Manova 1959, Duerr et al. 1982, and Dolan & Mathieu 2001), by X-ray surveys (Barrao et al. 2011, Franciosini & Sacco 2011), and infrared surveys (Bouy et al. 2009, Hernández et al. 2010). An extensive and unbiased spectroscopically confirmed census of the low-mass stars and brown dwarfs in the region is given by Bayo et al. (2011). Although some of these stars may have been born at the same time as the O and B stars, studies of other similar groups suggest that some of the stars are second-generation and only a few million years old. The densest subclusters of young stars are found near  $\lambda$  Ori itself, and in front of the small dense cloud Barnard 35.

The B35 molecular cloud (aka Lynds 1594) lies towards the projected interior of the  $\lambda$ -Ori ring and shows a pronounced cometary shape as seen in Figure 1. The “tail” of the comet extends for over a degree to the east of the B35 cloud core (Lada & Black 1976), directly away from the center of the  $\lambda$ -Ori OB subgroup. This morphology provides strong evidence for direct interaction between radiation fields and/or expansion of the HII region excited by the massive stars in this region. The famous star FU Orionis is located in the south-eastern wing of the B35 cloud, surrounded by a large reflection nebula (e.g., Herbig 1966). Early attempts to detect an embedded population at near- and far-infrared wavelengths were not successful (Lada & Wilking 1980, Lada et al. 1981). An overview of the literature on the  $\lambda$  Ori region is given by Mathieu (2008).

\* E-mail: reipurth@hawaii.edu

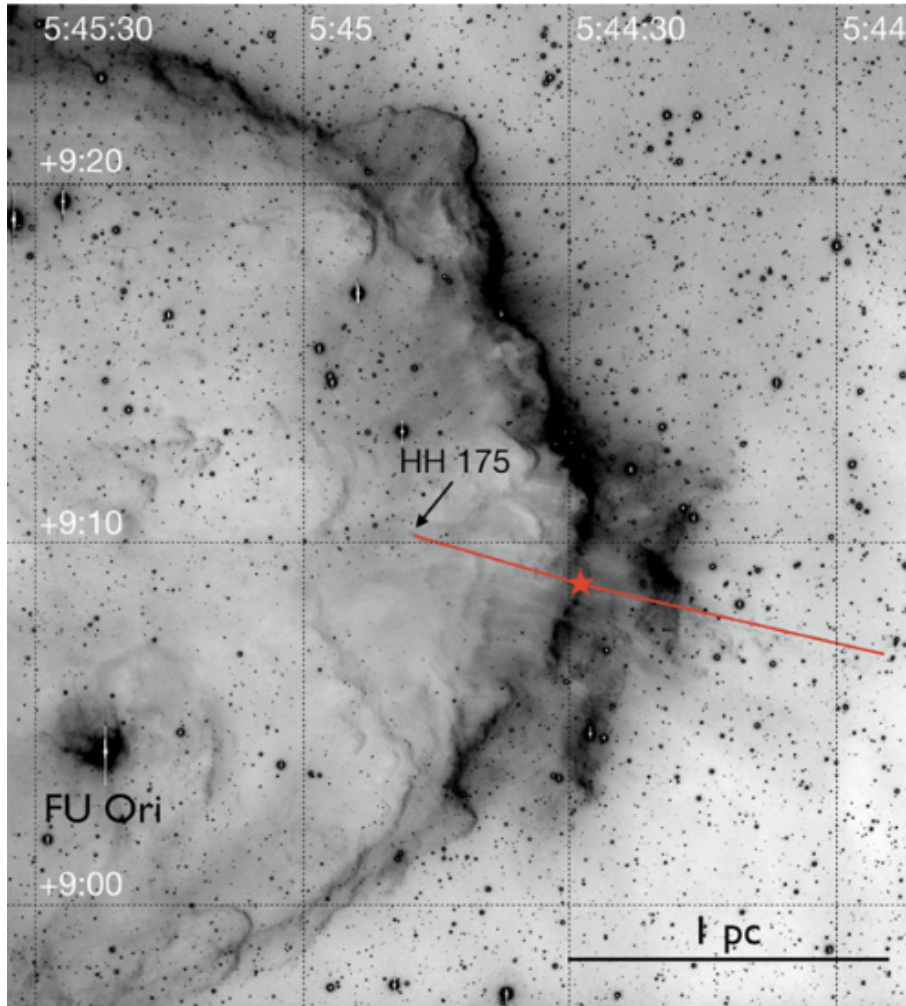


**Figure 1.** The cometary cloud B35 is facing the O-star  $\lambda$  Ori, and consequently has a prominent bright rim. The giant HH 175 flow is indicated together with its driving source.  $H\alpha$  image obtained with the Subaru telescope.

## 2 OBSERVATIONS

The B35 cloud was imaged with SuprimeCam on the Subaru 8m telescope at Mauna Kea under program 2005b-UH-53A. We used an  $H\alpha$  filter (N-A-L659) on Jan 4, 2006 and the exposure was  $5\times 6$  min in a seeing of about 0.95 arcsec. The [SII] image was obtained with the N-A-L671 filter on Jan 5, 2006 and the exposure was  $5\times 6$  min in a seeing of about 0.55 arcsec. The weather was clear.

JCMT observations were obtained under the University of Hawaii program m18bh13a and m19a16. Searches of the JCMT science archive generated additional data from 2007, 2010 and 2017. These data were also included in the reduction, but the bulk of the data came from 2018 and 2019.

The CO,  $^{13}\text{CO}$  and  $\text{C}^{18}\text{O}$  J=3-2 observations of B35 were obtained using the HARP array receiver and the auto-correlator ACSIS (Buckle et al. 2009). A  $900\times 900$  arcsecond area was mapped in CO J=3-2 using raster scanning. The line was observed with ACSIS using a bandwidth of 250 MHz and a resolution of 30.5 kHz or 0.026 km/s. This resolution has been smoothed to improve the noise level as required.  $^{13}\text{CO}$  and  $\text{C}^{18}\text{O}$  J=3-2 was observed at the same time by splitting the ACSIS into two 250 MHz sub-bands with a spectral resolution of 61 kHz or 0.052 km/s. Due to the higher opacity and weaker emission at  $^{13}\text{CO}$  and  $\text{C}^{18}\text{O}$  an area of  $300\times 210$  arcsecond

was mapped covering the central source area. Some of the archived data covered the full  $900\times 900$  arcsecond area. The data reduction was performed with the starlink *smurf* software (Jenness et al. 2008).

The SCUBA2 observations were 900 arcsec *pong* observations at 850 and 450  $\mu\text{m}$  (Holland et al. 2013). In addition a small amount of SCUBA2 data covering the central source was obtained from the archive. The data were reduced using the starlink *smurf* reduction package (Chapin et al. 2013). In addition to IRAS 05417+0907, only two other sources were detected at 850  $\mu\text{m}$ , namely the young stars V629 Ori and QR Ori.

## 3 RESULTS

### 3.1 Distance

In order to properly estimate physical properties of the HH 175 flow, the distance to B35 is important. Murdin & Penston (1977) derived a distance of  $440 \pm 40$  pc based on main-sequence fitting of 11 early-type stars in the  $\lambda$  Ori region. Subsequently, Dolan & Mathieu (2001) suggested a distance of  $450 \pm 50$  pc based on Strömgren photometry of OB stars in the region.

More recently, Zucker et al. (2019,2020) used Gaia distances of

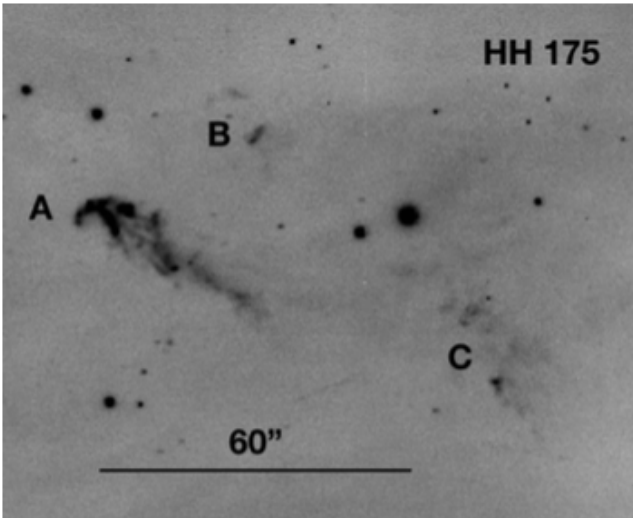


**Figure 2.** The HH 175 complex at the head of the eastern lobe of the outflow, as seen in a [SII] image. The main structures are labeled. The apex of the bright shock A is at 5:44:48.3 +9:10:15 (2000).

stars in front of and behind the  $\lambda$  Ori cloud, and determined a mean distance for seven sightlines of  $410 \pm 20$  pc.

We have obtained Gaia DR2 parallaxes for the 20 stars around  $\lambda$  Ori listed in Table 5 of Dolan & Mathieu (2001). One of these stars, HD 36267, is a binary with distances of 108 and 110 pc, and another, HD 35729, has a distance of 187 pc. We assume these 3 stars are foreground objects and hence reject them. By inverting the parallaxes of the remaining stars we derive a mean distance of 420 pc. From the cometary morphology of B35, it appears that it is seen from the side facing  $\lambda$  Ori, and we assume it is at the same distance as the central OB stars.

We have also obtained the Gaia distance to the nearby FU Ori, the brightest young star in B35, and find a distance of  $416_{-8}^{+9}$  pc, in excellent agreement with the above estimates. In the following we adopt a distance to B35 of 415 pc.

### 3.2 HH 175: Optical Imaging and Spitzer Data

HH 175 was discovered by Reipurth (1999). It has an elongated structure with a bright head, and several more knots adjacent to it, which are labeled in Figure 2. Interference filter images obtained in  $H\alpha$  and [SII] filters show that the object is weak in  $H\alpha$  but strong in [SII], indicating that the shock is weak. The morphology of HH 175 suggests that its driving source may lie to the WSW.

Figure 3 shows the region from HH 175 to the WSW in the optical and at  $4.5 \mu\text{m}$  as observed by Spitzer. The emission seen in the IRAC bands is mainly from thermal molecular hydrogen at non-LTE, although in cases where the  $4.5 \mu\text{m}$  emission is stronger (as appears to be the case for HH 175), additional emission is required, most probably from CO vibrational emission (e.g., Takami et al. 2010). It is immediately evident that the  $4.5 \mu\text{m}$  emission can be seen essentially all the way from the apex of HH 175 to a bright infrared source identified as IRAS 05417+0907, which is deeply embedded and not detected at optical wavelengths. The flow appears as a long tube that at its widest is about 40 arcsec ( $\sim 16,000$  AU) wide. Towards the apex, the flow breaks up and two small separate fingers are seen, reminiscent of the (much more) broken-up HH 2 working surface (e.g., Herbig & Jones 1981). The apex of each finger

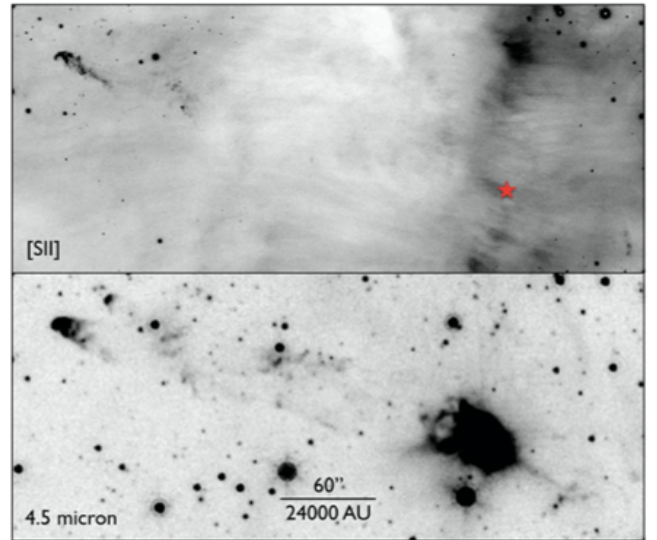


**Figure 3.** The eastern half of the HH 175 flow as seen in the optical ([SII]) and infrared ( $4.5 \mu\text{m}$ ). The red asterisk indicates the source location.

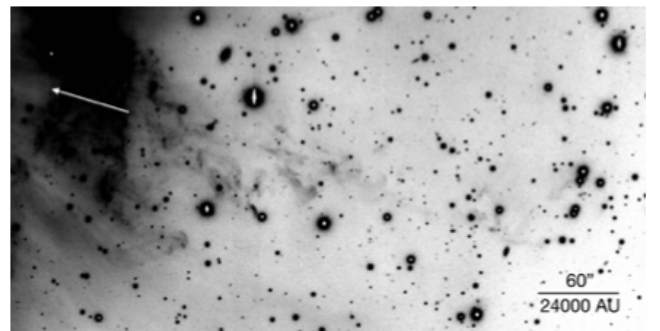


**Figure 4.** The western part of the HH 175 flow where it has burst out through the bright rim of the B35 cloud, as seen in the optical ( $H\alpha$ ). The multitude of scattered knots are designated as HH175W. The white arrow points to the source.

coincides with HH 175 A and B, respectively. It follows that HH 175 is just the front of a very long outflow, about 5 arcmin long, most of which is heavily obscured. At the distance of B35, this implies an extent of the eastern lobe of 0.6 pc. Assuming that the HH flow moves with a tangential velocity of  $\sim 100$  km/s, then the dynamical age of HH 175 is about 6,000 yr.

While the eastern side of the HH 175 flow is clearly seen in the optical and infrared images, the western side is very different. Only a little HH emission is visible immediately west of the source, one small group of knots can be distinguished in the lower right corner of Figure 3-top, and we denote it HH 175W. The difficulty in identifying HH emission here is partially because the flow is passing through the luminous bright rim of the B35 cloud with its disturbed emission structure. But when continuing beyond the edge of the molecular cloud, a complex of numerous knots and filaments appear, with the whole structure pointing back towards the IRAS source (Figure 4). We interpret this as a result of the flow bursting out of the molecular cloud and entraining and dragging gas and dust into the ionized zone. This is further discussed in Section 4.1.

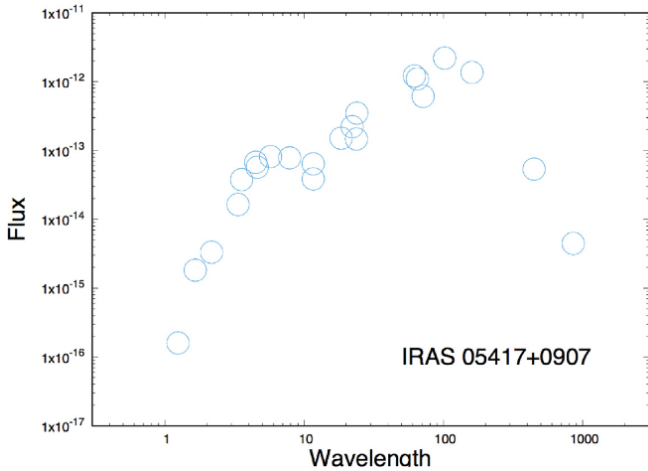


**Figure 5.** The energy distribution of IRAS 05417+0907 based on data from 2MASS, Spitzer, WISE, IRAS, Akari, and SCUBA-2. The flux values are listed in Table A1.

The overall length of the HH 175 flow from the apex of HH 175 in the east to the most distant H $\alpha$  fragment in the western lobe is 13.7 arcmin, corresponding to a projected extent of 1.65 pc at the distance of 415 pc.

### 3.3 The HH 175 Source

In Figure 5 we show the spectral energy distribution (SED) of the source IRAS 05417+0907 based on observations from PanSTARRS, 2MASS, Spitzer, WISE, IRAS, Akari, and our own SCUBA2 sub-mm data. The SED rises up to a peak around 100  $\mu\text{m}$ , indicating an envelope with a temperature around 30 K. A clear silicate dust absorption feature is seen around 10  $\mu\text{m}$ . IRAS 05417+0907 is a low-luminosity source, Morgan et al. (2008) suggested a  $L_{\text{bol}} \sim 6$  calculated from a blackbody fit to IRAS and SCUBA2 450 and 850  $\mu\text{m}$ . The more detailed SED presented here yields a luminosity of 15  $L_{\odot}$  at the adopted distance of 415 pc. The luminosity and SED indicate that the object is a low-mass Class I protostar. The object is also listed as 2MASS J05443000+0908573 with  $H=15.91$  and  $K=12.40$ . We have examined archival Spitzer images and in Figure 6 show the source and its environment from 3.6 to 24  $\mu\text{m}$ . It is readily seen that the source is not a single object, but forms a small multiple system. We have labeled the various components A-E, and note that whereas the 2MASS source (labeled C) is the dominant source at 3.6  $\mu\text{m}$ , another source to the WSW increases in brightness at longer wavelengths, until it dominates the group at 24  $\mu\text{m}$ . The above luminosity determination is likely to include several of these sources. The coordinates of the 5 sources are listed in Table 1.

Connelley et al. (2008) obtained a L-band image of IRAS 05417+0907 in a survey for protostellar binaries, and they found source C to be a close binary with a separation of 1.2 arcsec. Figure 7 shows an L-band image of the source region, based on data from Connelley et al. (2008). The exposure is brief in order to not saturate the brightest source. It is seen that IRAS 05417+0907 is a quadruple system, arranged in a non-hierarchical configuration. As mentioned above, the source detected by IRAS is source A, which is barely detected in this short exposure.

Herschel observed the region, and Figure 8 shows a comparison of the apex of the B35 cloud as imaged with Subaru in a [SII] filter, with Spitzer at 24  $\mu\text{m}$  and with Herschel at 100  $\mu\text{m}$ . Known young

**Table 1.** Coordinates of IRAS 05417+0907 Trapezium Sources (from Spitzer 3.5  $\mu\text{m}$  image)

Source	$\alpha_{2000}$	$\delta_{2000}$
A	5:44:29.27	+09:08:52.6
B	5:44:29.24	+09:08:56.7
C1	5:44:29.96	+09:08:57.0
C2	5:44:29.92	+09:08:55.9
D	5:44:30.86	+09:08:26.3
E	5:44:31.64	+09:08:57.9

stars from the Dolan & Mathieu (2001) catalog are marked with red circles. Comparing the images it is evident that IRAS 05417+0907 is currently the only protostar at the apex of the cloud. The B35 cloud is located at the eastern edge of the HII region around  $\lambda$  Ori, and its cometary shape and bright rims testifies to the effect of the central OB stars. It appears that IRAS 05417+0907 is another case of triggered star formation (e.g., Sugitani et al. 1991).

IRAS 05417+0907 source A was detected at 6 cm with the VLA by Terebey et al. (1992), who also detected two highly variable H $_2$ O masers located within a fraction of an arcsecond from the position of source A given in Table 1. Additional detections were made by Claussen et al. (1996). We have observed the source region with SCUBA2 on the JCMT at 450 and 850  $\mu\text{m}$ , and found no other submm sources in the field (Figure 9). IRAS 05417+0907 appears as a bright unresolved source with a conical nebula to the north-east along the flow axis, suggesting that this is the outflow cavity illuminated and heated by the jet. Perotti et al. (2021) have carried out a major near-infrared and mm-study of the environment of IRAS 05417+0907 in order to calculate the gas-to-ice ratio for CO and CH $_3$ OH, thus casting light on how these solid-state molecules on dust grains are converted into the gas phase.

Finally, we examine the evidence for youth of the components of the IRAS 05417+0907 components. The detection of A, C, and D at 100  $\mu\text{m}$  combined with the IRAS colors show that they are young embedded protostars. Additionally, Connelley et al. (2007) detected reflection nebulae around C and D. The detection of B out to 24  $\mu\text{m}$  and E out to 8  $\mu\text{m}$  are indicative but not proof that they are young.

The dynamical evolution of the IRAS 05417+0907 trapezium and its relation to HH 175 is discussed in Section 4.2.

### 3.4 Cloud Structure and Molecular Outflow

A low-resolution mm-study of B35 was carried out by Lada & Black (1976), who found that the  $^{12}\text{CO}$  column density peaks behind the western ionization front. Myers et al. (1988) and Benson & Myers (1989) made a small low-resolution map in  $^{12}\text{CO}$  and NH $_3$  around the IRAS 05417+0907 source, and discovered an energetic bipolar molecular outflow emanating from a dense core. Additional low-resolution  $^{12}\text{CO}$  observations were made by Qin & Wu (2003). Craigon (2015) performed a more detailed mm study of B35 and the molecular outflow and suggested a correlation between the gas temperature and PAH emission consistent with photoelectric heating.

Our JCMT/HARP observations form the deepest and most detailed mm study of B35 to date, for technical details see Section 2. A mosaic of 12 channel maps with 8'' resolution (pixel size 6'') in  $^{12}\text{CO}$  J=3-2, covering almost all of B35, is presented in Figure 10. The velocity range shown covers  $9.25 < v_{\text{LSR}} < 15.25$  km/sec. The bulk of the molecular cloud is seen between 11.75 and 12.75 km/sec, and we adopt a mean velocity of 12.25 km/sec as the average cloud velocity. The enhancement of  $^{12}\text{CO}$  emission behind the ionization-shock

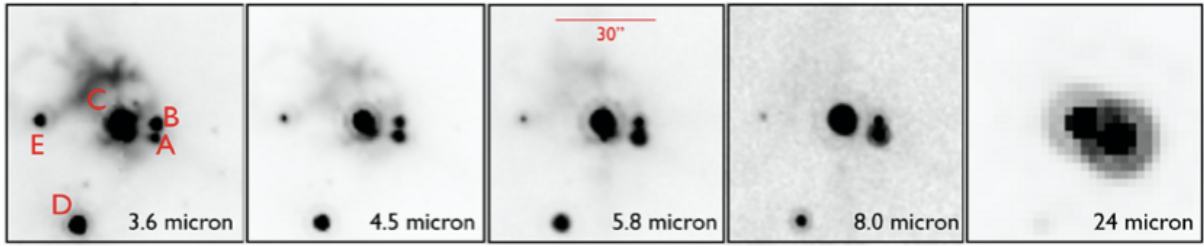


**Figure 6.** Spitzer images of the source. Each panel is slightly larger than one arcmin wide. Source A is the dominant source at long wavelengths.

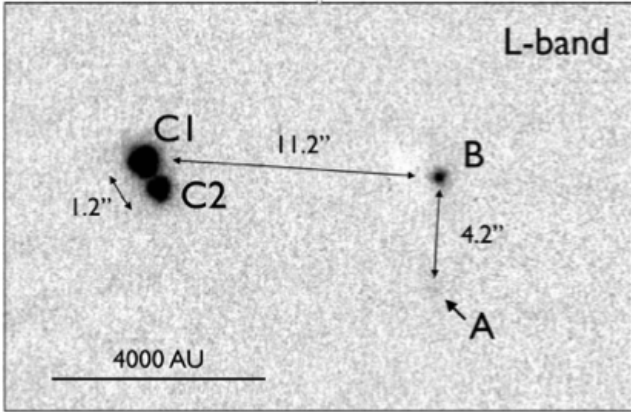


**Figure 7.** An L-band image of IRAS 05417+0907 showing the components of the multiple system. The source A, which dominates at longer wavelengths, is barely detected in this exposure which was kept short to not saturate the bright binary. Image from Connelley et al. (2008).

front is most clearly seen in the 11.75-12.25 km/s panel. It also appears that there is a slight asymmetry in the velocity distribution, such that the southern part of B35 moves towards the observer while the northern part tends to move away. The velocity gradient is about 1 km/sec from North to South. The  $C^{18}O$  J=3-2 contour map in Figure 11 shows that the B35 cloud is highly fragmented, and that the HH 175 source is located in the very densest part of the B35 cloud (the colored part of the figure is from the 450  $\mu$ m SCUBA2 map).

To derive a cloud mass, we assume a distance of 415 pc and a  $N(H_2)/N(^{13}CO)$  ratio of  $7.1 \times 10^5$  (Frerking et al. 1982). We can derive a mass assuming we know the excitation temperature  $T_{ex}$  and that  $^{13}CO$  is optically thin (Mangum & Shirley 2015). The excitation temperature will vary across the map and along the line-of-sight which passes through both the warm skin of the cloud and the colder interior regions and, additionally,  $^{13}CO$  is likely partially optically thick. Without detailed knowledge of these issues, we have chosen to adopt an excitation of 25 K along the northwestern edge and of 16 K in the eastern interior of the cloud based on the  $^{13}CO$  excitation temperature map derived by Craigm (2015). Using these two uniform temperatures we find a mass of  $36 M_{\odot}$  for B35. The uncertainty in this determination is considerable due to the above mentioned assumptions. As a comparison we get 39 and  $29 M_{\odot}$  for excitation temperatures of 16 and 25 K, respectively, assuming they are uniform across the cloud.

Figure 10 very clearly shows the molecular outflow emanating from IRAS 05417+0907 at a position angle of  $\sim 72^\circ$ . As already noted by Craigm (2015) the outflow is significantly collimated. Figure 12 outlines the blue and red lobes overlaid on the deep Suprime-

Cam image. The figure shows that the eastern lobe is very extended, reaching almost out to HH 175. In contrast, the western lobe is short and stubby. This is well understood when compared with the extinction seen in the optical image: the driving source is located at the western edge of a dense rim, through which the flow burrows until emerging on the eastern side of the rim. As it escapes at the cloud rim it no longer passes through dense gas to entrain, and hence does not reach all the way to the HH object. Similarly for the western lobe, which escapes into the tenuous ambient medium in front of B35. The eastern lobe shows both strong blue and red emission, indicating that the flow axis is very close to the plane of the sky, in agreement with the results of Craigm (2015). Figure 13 shows the line profiles of  $^{12}CO$ ,  $^{13}CO$ , and  $C^{18}O$  towards the peak emission and towards the source.

Due to the flow having a very low angle of inclination to the plane of the sky, there is substantial overlap in velocity between the outflow and the ambient cloud. This is an obstacle to an estimate of the outflow mass. Craigm (2015) subtracts a scaled quiescent cloud line profile centered at 12.42 km/s to remove the ambient cloud contribution from the flow estimates. However, looking at the spectral lines in Figure 13, their profiles are complex and towards the source  $C^{18}O$  covers a wider interval than the ambient cloud and is centered below 12.42 km/s. We have instead integrated the flow over selected velocity intervals. The red and blue line wings were integrated over a sequence of velocity intervals ending closer and closer to the line center. The resulting maps were then spatially integrated over the flow region. This was done both for the  $^{12}CO$  and  $^{13}CO$  J=3-2 lines. The ratio between integrated  $^{12}CO$  and  $^{13}CO$  values is about 70 in the red wing until the lower edge in the velocity range reaches 13.5 km/s. Below 13.5 km/s the ratio begins to drop fast. We assume this is due to contribution from the ambient cloud and cloud core. The blue wing is partially optically thick, the ratio between integrated  $^{12}CO$  and  $^{13}CO$  values are about 12 until the upper edge in the velocity range reaches 11.0 km/s at which point it starts to drop. Hence we have adapted 11.0 km/s to 13.5 km/s as the region mostly affected by the ambient cloud, and therefore exclude this when integrating the outflow over velocity.

Outflow masses for the two lobes have been calculated for the following regions: a rectangular area with width of 250'' and tilted 28.5 degrees following the flow area for 310'' towards east-northeast from Source A and 140'' towards west-southwest from Source A.

The flow mass has been calculated using the  $^{13}CO$  transition, since  $^{12}CO$  is likely optically thick and the line profiles in Figure 13 show signs of self absorption. Assuming that the  $^{13}CO$  line is optically thin and adopting an excitation temperature of 25 K, the large eastern lobe has a total mass of  $0.60 M_{\odot}$  (blue  $0.54 M_{\odot}$ , red  $0.06 M_{\odot}$ ) and the smaller western lobe has a total mass of  $0.37 M_{\odot}$  (blue  $0.37 M_{\odot}$ , red  $0.002 M_{\odot}$ ). In total, we find an outflow mass (lower limit) of  $\sim 0.97 M_{\odot}$ , which compares well with the mass of  $0.86 M_{\odot}$  derived by Myers et al. (1988). For excitation temperatures of 35 K and 16 K,

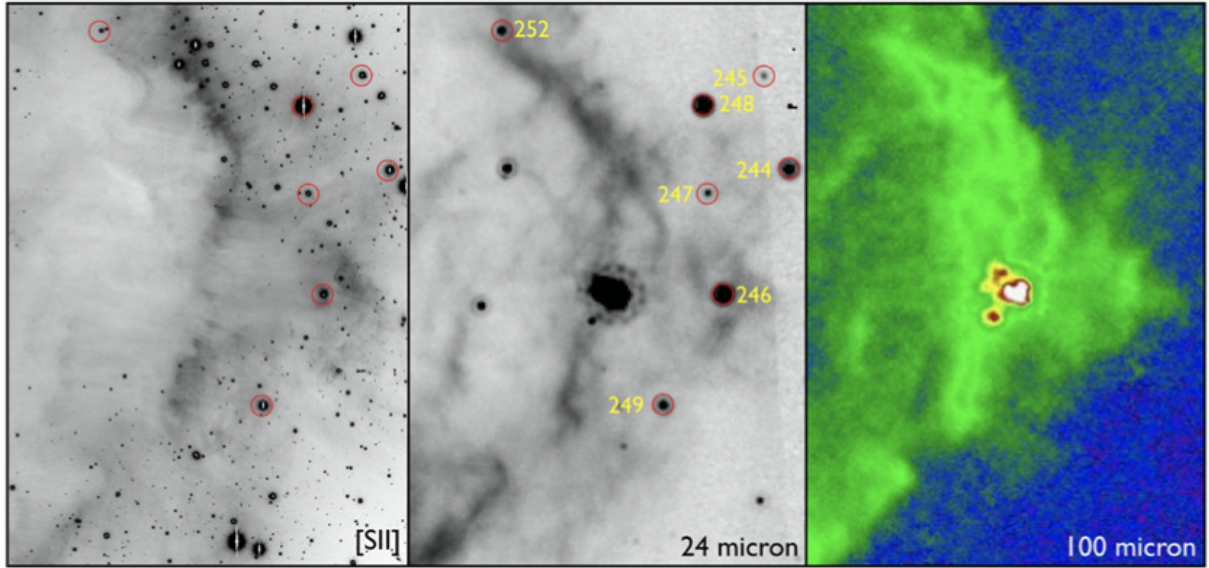


**Figure 8.** A multi-wavelength panel featuring the apex of the B35 cloud in a Subaru [SII] filter, and Spitzer MIPS 24  $\mu\text{m}$  and Herschel 100  $\mu\text{m}$  maps. The center image has known pre-main sequence stars marked, labeled following the catalog of Dolan & Mathieu (2001). The Herschel panel shows the small IRAS 05417+0907 trapezium, revealing that it is currently the only protostars embedded in the cloud. Each figure is 6 arcmin wide.

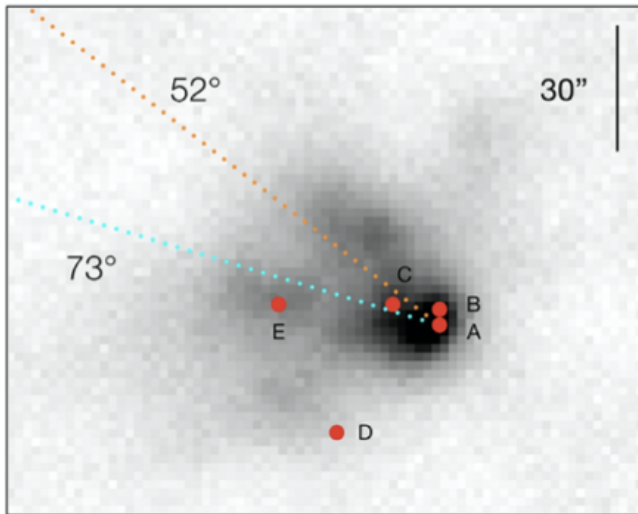


**Figure 9.** The HH 175 driving source IRAS 05417+0907 observed at 450  $\mu\text{m}$  with SCUBA-2. What appears to be the dusty walls of an outflow cavity is opening away from the source. The direction to the HH 175 bow shock is indicated as a turquoise dotted line, and the direction to the peak intensity of the molecular outflow is marked in orange.

lower limits for the total flow masses are  $0.93 M_{\odot}$  and  $1.30 M_{\odot}$ , respectively. Given the many physical and geometric uncertainties involved, it is difficult to estimate the uncertainty of these numbers, but it appears that the mass of the HH 175 molecular outflow is in the same range as for many other molecular outflows (e.g., Bally et al. 1999, Lee et al. 2002).

### 3.5 On the Nature of HH 175X

While examining the deep SuprimeCam images, we noted a small jet-like feature, here named HH 175X and marked in Figure 12. As

can be seen in Figure 14, HH 175X has the morphology of a well collimated jet, bright in [SII] emission, with 4-5 well-defined knots stretching over 7 arcsec, corresponding to 2800 AU, and an off-axis knot further away.

Under normal circumstances we would not hesitate to identify this as another small jet in a star forming cloud. But in this case the object is located within the lobe of a giant HH flow bursting out through the torn fabric of a cloud. Thus it could well be a fragment like the many other small shocks and photoionized clumps in the outflow lobe. Speaking against this, however are the following facts: (1) HH 175X stands out as by far the brightest of these small scale shocks; (2) The structure of well aligned knots would be unusual for a random filament; (3) The jet knots appear to emerge from a faint star; (4) The object is located within the bright rim of a dense cloud that is known to have recently spawned numerous low-mass stars (Dolan & Mathieu 1999, 2001, 2002).

Each of these alone would not be sufficient to warrant much attention, but taken together it seems at least possible that this could be a new small HH jet.

HH 175X is not precisely aligned with the star at its eastern end. Closer examination shows that the pointspread function of the star differs from those of the surrounding stars, and is elongated at a PA of about  $45^{\circ}$  towards the end of the jet. This suggests a companion at  $\sim 0.33$  arcsec, corresponding to about 130 AU. The coordinates of this star at the end of HH 175X are (2000): 5 44 19.56 +09 07 35.6. The faint star is not detected by 2MASS, but is (very) weakly seen in all four Spitzer IRAC channels. It is thus not showing signs of significant circumstellar material.

For the time being, we think it most likely that HH 175X is another shocked fragment in this outflow, but further observations, in particular of proper motions, are needed to fully settle this issue.

## 4 DISCUSSION

The recognition and study of giant HH flows is important, because they provide insight into a number of physical processes in star for-

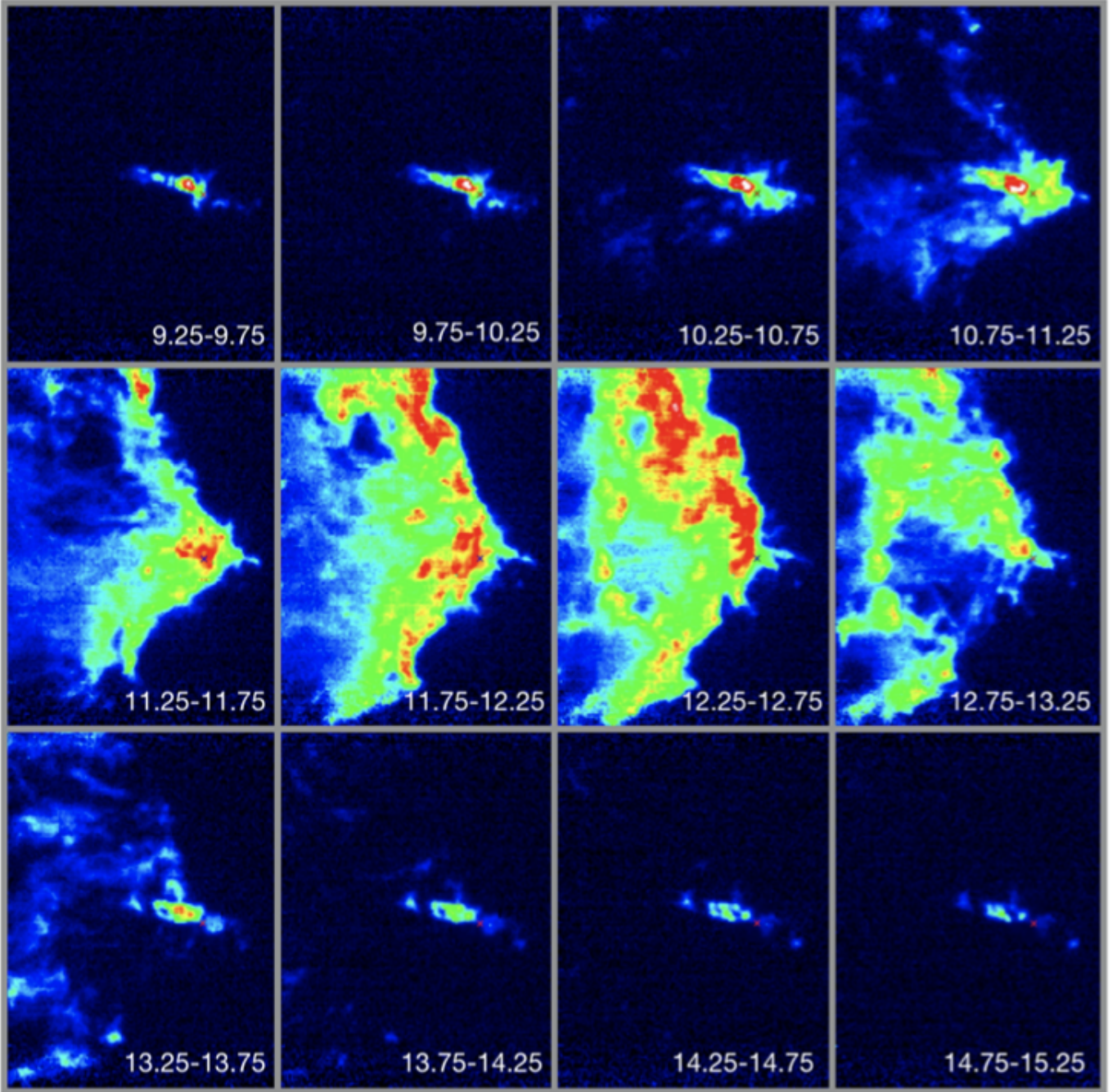


**Figure 10.** A mosaic of 12 panels showing B35 and the HH 175 molecular outflow in  $^{12}\text{CO}$  from blueshifted (top left) to redshifted (bottom right). The  $v_{LSR}$  velocities spanned by each panel is indicated. The panels are 18.4 arcmin high, corresponding to 2.25 pc.

mation. Because their dynamical time scales can be several times  $10^4$  yr, they provide a fossil record of the most recent evolution and accretion history of their driving sources. Multi-epoch imaging and spectroscopic analyses indicate variability in their ejection directions and velocities. Detailed studies of HH flows indicate a systematic decrease in their space velocities with time (e.g., Devine et al. 1997) which is interpreted as a deceleration of the ejecta as they penetrate the ambient medium (e.g., Cabrit & Raga 2000). Because HH flows transfer energy and momentum into their ambient medium,

they may be an important contribution to the maintenance of turbulence in molecular clouds. Finally, because fast shocks will dissociate molecules, giant HH flows can result in a chemical rejuvenation of clouds in star forming regions.

#### 4.1 Observations and Models of Breakout

Parsec-scale outflows have dimensions much larger than the cloud cores in which they originate. As a consequence, giant outflows

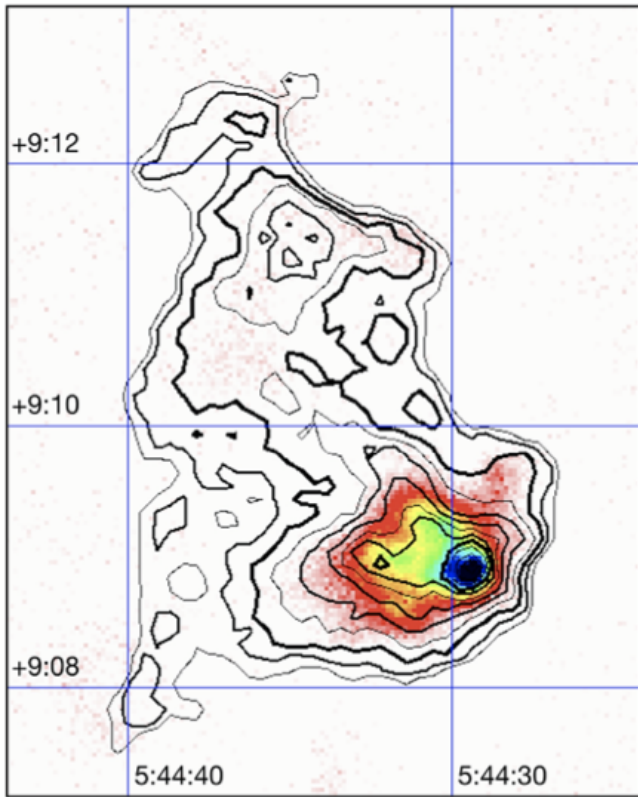


**Figure 11.** The structure of the B35 cloud observed in  $C^{18}O$  overlaid on a color-map of the same region observed at  $450\mu m$  with SCUBA2 on JCMT. It is evident that the little cluster around IRAS 05417+0907 is the only actively star forming region in B35.

usually punch out of their birth clouds and inject energy, momentum, and mass into the intercloud medium. In regions of massive star formation, this implies that the flows and the entrained gas they drag along are bathed in UV radiation.

HH jets that are formed from stars located outside their nascent clouds may, in addition to the emission from shocks, show emission from photoionization (Cernicharo et al. 1998, Reipurth et al. 1998). Similarly, a molecular outflow that entrains gas while embedded and which breaks out from the neutral cloud into an HII region will become photoionized. Bally et al. (2002) found two such cases while studying the S140 region. S140 has a well-defined and rather sharp interface between ionized and neutral gas and Bally et al. found two flows, HH 616 and HH 617, bursting out of the dense molecular gas. Subsequently, Reipurth et al. (2003) identified another case, where an outflow, HH 777, breaks out of the IC 1396N cometary globule. Since then, a few more cases have been found, in particular the HST images of the HH 902 flow in Carina show the phenomenon well (e.g. Smith et al. 2010). The nature of such blow-outs from cloud cores were investigated through numerical simulations by Raga & Reipurth (2004). By varying physical parameters of flow and cloud core an overview of the properties of such blowout was established. The working surfaces of the flow essentially act as neutral clumps which are irradiated by the impinging ionizing photons. The emission of the flows is therefore dominated by the impinging photon field rather than by dynamical properties of the working surfaces. Evidently, once the jet emerges from its cloud core into the tenuous intercloud medium, it runs out of material to entrain. It follows that the scattered

fragments found in the western lobe of HH 175 have been dragged out from the cloud interior. The western lobe is significantly longer than its eastern counterpart which has penetrated the cloud, as one would expect from momentum conservation.

For reasons that are not clear, most outflows that break out of their birth clouds do not show evidence of such fragments dragged out of the cloud. An example is the HH 111 jet, whose eastern lobe plunges through the cloud, while the western lobe flows directly from the cloud core into a void, without any evidence of swept-up cloud material.

#### 4.2 Giant HH Flows and Multiple Energy Sources

A very high fraction of multiplicity in the sources of giant HH flows was noted by Reipurth (2000), and many more giant flows with multiple driving sources have been noted by now. It is possible that there is a causal link between multiplicity and the giant HH flows. It is well known that non-hierarchical triple systems are unstable, and following a close triple encounter during which energy and momentum can be exchanged, this leads either to the formation of a hierarchical triple system with a close binary and a distant third component, or the third body is escaping, leaving behind a binary (Valtonen & Mikkola 1991).

Most stars are born in small multiple systems, which decay (e.g., Sterzik & Durisen 1998). In case the body that escapes has not had time to gain sufficient mass to achieve hydrogen burning, then it remains a brown dwarf (Reipurth & Clarke 2001).

The binary that remains after a triple decay becomes highly eccentric and is tightened in the process. If it furthermore moves in a dissipative gas environment, it may spiral in, leading to a spectroscopic binary or even a merger (Bate 2002, Reipurth et al. 2014).

These dynamical processes lead to significant disk-disk interactions at periastron, and result in accretion events with a consequent burst of outflow activity (e.g., Tofflemire et al. 2017). We can thus understand the formation of giant HH flows as a consequence of the evolution of a newly formed binary: when a newly born triple system undergoes a close triple encounter during which their disks violently collide, then a major outflow event is initiated. The resulting binary will additionally produce accretion/outflow episodes during subsequent periastron passages, which will become increasingly frequent as the binary spirals in. Eventually the stars are so close, of the order of  $\sim 10$  AU or so, that a jet is formed with multiple closely spaced knots.

In the case of HH 175, we clearly see that the source forms a small multiple system. In accordance with the scenario outlined above, we thus postulate that source A is now a close binary in the process of spiraling in, following a dynamical interaction with one or more of the other stars in the system about 6,000 yr ago, the estimated dynamical age of HH 175. The mean terminal velocity of ejectees from a low-mass triple system is 1.1 km/sec (Reipurth et al. 2010), indicating that an ejected companion would be of the order of a few arcseconds away from source A. The separation of source A and B is 4 arcsec, suggesting a possible connection to the event that formed the HH 175 flow.

## 5 CONCLUSIONS

We have studied the region of the newly discovered HH 175 object in the B35 cloud associated with the  $\lambda$  Ori region, and have reached the following conclusions:

1. Wide-field optical images together with Spitzer images reveal

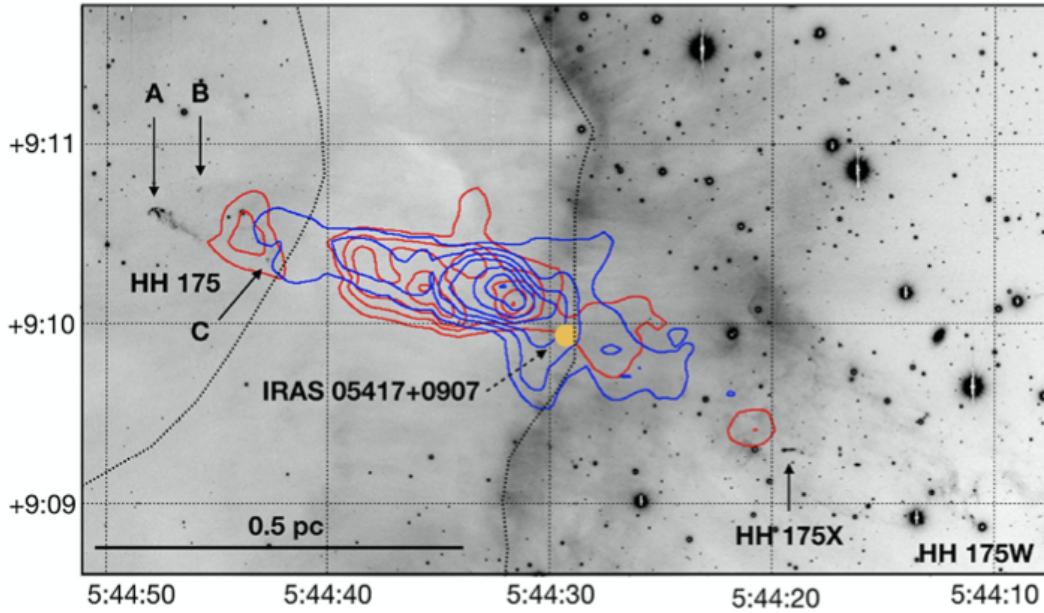


**Figure 12.** The molecular outflow driven by IRAS 05417+0907 plotted on a [SII] optical image. The eastern lobe is prominent where the flow burrows through the cloud, whereas the western lobe is much less prominent as it breaks out of the cloud. The dense ridge observed in CO is indicated by dotted lines.

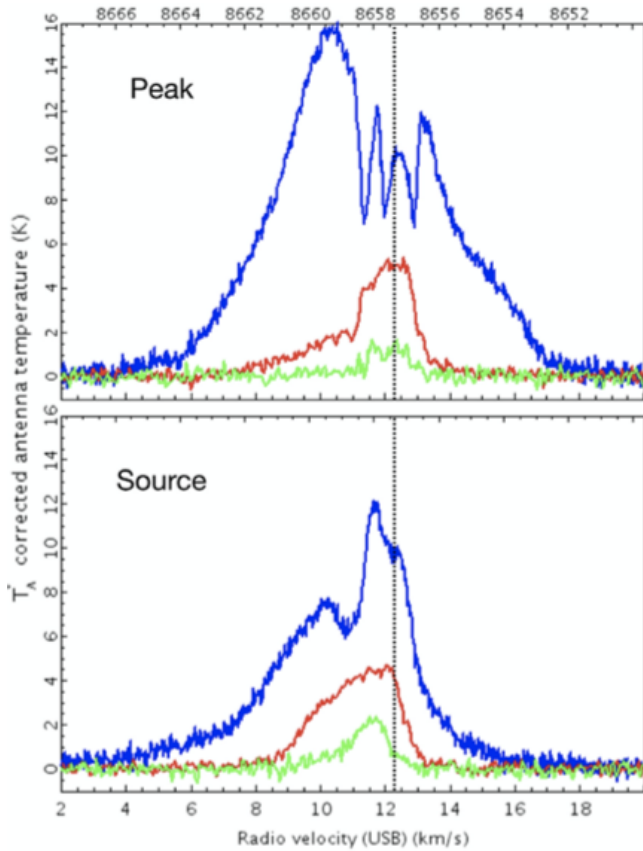


**Figure 13.** Line profiles observed with JCMT towards two regions in the HH 175 molecular outflow. On top is the pointing towards the region with strongest emission (5:44:31.8 +9:09:19 - 2000) just ENE of the source (see Figure 12), and below is the emission towards the source (5:44:29.8 +9:08:54 - 2000). Blue is  $^{12}\text{CO}$  J=3-2, red is  $^{13}\text{CO}$  J=3-2, and  $\text{C}^{18}\text{O}$  J=3-2 is green. The dotted line indicates the mean rest-velocity 12.25 km/sec of the B35 cloud.

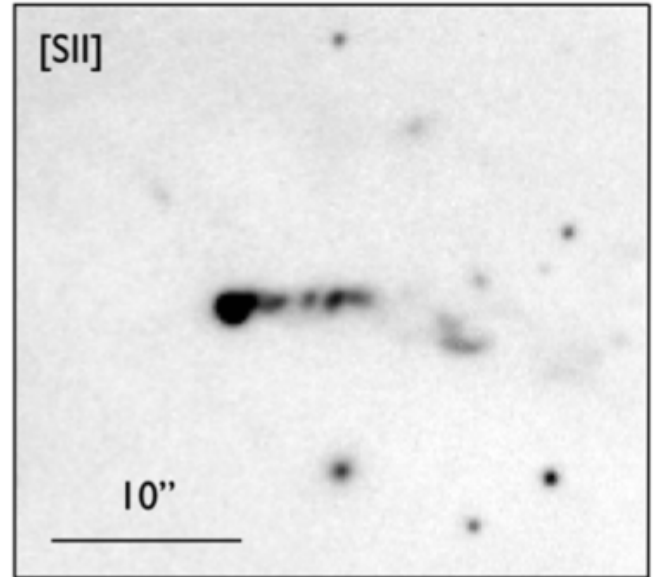


**Figure 14.** HH 175X as seen in a [SII] image from the Subaru telescope. HH 175X is located within the western lobe of the giant HH 175 flow, and may be a shocked fragment of the outflow, but because of its collimated morphology and unusual brightness it cannot be excluded that it is an independent jet. The star at the eastern end of HH 175X is at 5:44:19.5 +09:07:35 (2000).

a giant outflow with an extent of 1.65 pc, in which HH 175 is the terminal shock of the eastern lobe, whereas the western lobe breaks out of the face of the B35 cloud. For an assumed tangential velocity of 100 km/sec, the dynamical age of the outflow is  $\sim 6,000$  yr.

2. The driving source of the HH 175 flow is IRAS 05417+0907, an embedded Class I source which in Spitzer images resolve into a multiple system with at least 6 components.

3. Our  $^{12}\text{CO}$  J=3-2,  $^{13}\text{CO}$  J=3-2, and  $\text{C}^{18}\text{O}$  J=3-2 maps of the entire B35 cloud show that the IRAS source is embedded in a large dense cloud core and that the B35 cloud is highly fragmented.

4. The  $^{12}\text{CO}$  map reveals a major molecular outflow coinciding with the optical/IR flow. Both the eastern and western lobes show blue and red high-velocity wings, indicating that the outflow lies almost in the plane of the sky.

5. The HH 175 flow adds to the increasing number of multiple systems found to drive a giant HH flow. We argue that the HH 175 giant flow is the result of chaotic motions in an unstable non-hierarchical newborn stellar system, during which close periastron passages lead to major disk disturbances that lead to accretion events which again drive strong outbursts of outflow activity.

## ACKNOWLEDGEMENTS

We thank Giulia Perotti and Helen Fraser for drawing our attention to the thesis by Alison Craigon, and Michael Connelley for providing the image in Figure 7. We also thank an anonymous referee for helpful comments. Based in part on data collected at the Subaru Telescope, which is operated by the National Astronomical Observatory of Japan (NAOJ). Thanks are due to the Subaru staff, in particular Miki Ishii and Hisanori Furusawa (SuprimeCam) for excellent and dedicated support during the observations. We are grateful to Nobunari Kashikawa for permission to use his [SII] filter. The James Clerk Maxwell Telescope is operated by the East Asian Observatory on behalf of The National Astronomical Observatory of Japan; Academia Sinica Institute of Astronomy and Astrophysics; the Korea Astronomy and Space Science Institute; the Operation, Maintenance and Upgrading Fund for Astronomical Telescopes and Facility Instruments, budgeted from the Ministry of Finance (MOF) of China and administrated by the Chinese Academy of Sciences (CAS), as well as the National Key R&D Program of China (No. 2017YFA0402700). Additional funding support is provided by the Science and Technology Facilities Council of the United Kingdom and participating universities in the United Kingdom and Canada. Program ID M18BH13A. The JCMT archive is hosted by the Canadian Astronomy Data Center. This work is based in part on observations made with the Spitzer Space Telescope, which is operated by the Jet Propulsion Laboratory, California Institute of Technology under a contract with NASA. This paper has used archival data from the Herschel mission. Herschel is an ESA space observatory with science instruments provided by European-led Principal Investigator consortia and with important participation from NASA. This research has made use of the SIMBAD database, operated at CDS, Strasbourg, France, and of NASA's Astrophysics Data System Bibliographic Services.

## DATA AVAILABILITY STATEMENT

The data underlying this article will be shared on reasonable request to the corresponding author.

## REFERENCES

Bally, J. 2016, *Ann. Rev. Astron. Astrophys.* 54, 491  
 Bally, J., Reipurth, B., Lada, C.J., Billawala, Y. 1999, *AJ*, 117, 410  
 Bally, J., Reipurth, B., Walawender, J., Armond, T. 2002, *AJ*, 124, 2152  
 Barrado, D., Stelzer, B., Morales-Calderón, M. et al. 2011, *A&A*, 526:A21  
 Bate, M.R., Bonnell, I.A., Bromm, V. 2002, *MNRAS*, 336, 705

Bayo, A., Barrado, D., Stauffer, J. et al. 2011, *A&A*, 536:A63  
 Benson, P.J. & Myers, P.C. 1989, *ApJS*, 71, 89  
 Bouy, H., Huéramo, N., Barradi y Navascués, D. et al. 2009, *A&A*, 504:199  
 Buckle, J. V., Hills, R. E., Smith, H. et al. 2009, *Mon. Not. R. Astron. Soc.* 399, 1026  
 Cabrit, S. & Raga, A.C. 2000, *A&A*, 354, 667  
 Cernicharo, J., Lefloch, B., Cox, P. et al. 1998, *Sci*, 282, 462  
 Chapin, E.L., Berry, D.S., Gibb, A.G. et al. *MNRAS*, 430, 2545  
 Claussen, M.J., Wilking, B.A., Benson, P.J. et al. 1996, *ApJS*, 106, 111  
 Connelley, M.S.C., Reipurth, B., Tokunaga, A.T. 2007, *AJ*, 133, 1528  
 Connelley, M.S.C., Reipurth, B., Tokunaga, A.T. 2008, *AJ*, 135, 2496  
 Conti, P.S. & Leep, E.M. 1974, *ApJ*, 193, 113  
 Craigon, Alison M. 2015, PhD thesis, University of Strathclyde, Glasgow, [pdf]  
 Devine, D., Bally, J., Reipurth, B., Heathcote, S. 1997, *AJ*, 117, 2919  
 Dolan, C.J. & Mathieu, R.D. 1999, *AJ*, 118, 2409  
 Dolan, C.J. & Mathieu, R.D. 2001, *AJ*, 121, 2124  
 Dolan, C.J. & Mathieu, R.D. 2002, *AJ*, 123, 387  
 Duerr, R., Imhoff, C.L., Lada, C.J., 1982, *ApJ*, 261, 135  
 Franciosini, E. & Sacco, G.G. 2011, *A&A*, 530:A150  
 Frerking, M.A., Langer, W.D. & Wilson, R.W. 1982, *ApJ*, 262, 590  
 Haro, G., Iriarte, B., Chavira, E., 1953, *Bol. Tonantzintla y Tacubaya*, No. 8, 3  
 Heiles, C. & Habing, H.J. 1974, *A&A Supp.* 14, 1  
 Herbig, G.H. 1966, *Vistas in Astronomy*, 8, 109  
 Herbig, G.H. & Jones, B.F. 1981, *AJ*, 86, 1232  
 Hernández, J., Morales-Calderon, M., Calvet, N. 2010, *ApJ*, 722, 1226  
 Holland, W.S., Bintley, D., Chapin, E.L. et al. 2013, *MNRAS*, 430, 2513  
 Jenness T., Cavanagh B., Economou F., Berry D.S., 2008, in *Argyle R.W., Bunclark P.S., Lewis J.R., eds, Astronomical Society of the Pacific Conference Series Vol. 394, Astronomical Data Analysis Software and Systems XVII*. p. 565  
 Joy, A.H. 1949, *ApJ*, 110, 424  
 Lada, C.J. & Black, J.H. 1976, *ApJ*, 203, L75  
 Lada, C.J. & Wilking, B.A., 1980, *ApJ*, 242, 1056  
 Lada, C.J., Thronson, H.A., Smith, H.A. et al. 1981, *ApJ*, 251, L91  
 Lee, C.-F., Mundy, L.G., Stone, J.M., Ostriker, E.C. 2002, *ApJ*, 576, 294  
 Maddalena, R.J. & Morris, M., 1987, *ApJ*, 323, 179  
 Maddalena, R.J., Morris, M., Moscowitz, J., Thaddeus, P., 1986, *ApJ*, 303, 375  
 Mangum, J.G. & Shirley, Y.L. 2015, *PASP*, 127, 266  
 Manova, G.A. 1959, *Soviet Astron.*, 3, 188  
 Mathieu, R.D. 2008, in *Handbook of Star Forming Regions Vol. I. The Northern Sky*, ASP Monographs, Ed. Bo Reipurth, p. 757  
 Morgan, L.K., Thompson, M.A., Urquhart, J.S., White, G.J. 2008, *A&A*, 477, 557  
 Murdin, P. & Penston, M.V., 1977, *MNRAS*, 181, 657  
 Myers, P.C., Heyer, M., Snell, R.L., Goldsmith, P.F. 1988, *ApJ*, 324, 907  
 Perotti, G., Jørgensen, J.K., Fraser, H.J., Suutarinen, A.N., Kristensen, L.E., Rocha, W.R.M., Bjerkeli, P., Pontoppidan, K.M. 2021, *A&A*, in press  
 Qin, S.-L. & Wu, Y.-F. 2003, *Chin. Jour. Astron. Astrophys.*, 3, 69  
 Raga, A.C. & Reipurth, B. 2004, *Rev. Mex. Astron. Astrofis.* 40, 15  
 Reipurth, B. 1999, *A general catalog of Herbig-Haro objects*, 2. edition, <http://vizier.u-strasbg.fr/viz-bin/VizieR?-source=HH>  
 Reipurth, B. 2000, *AJ*, 120, 3177  
 Reipurth, B. & Bally, J. 2001, *Ann. Rev. Astron. Astrophys.* 39, 403  
 Reipurth, B. & Clarke, C.J. 2001, *AJ*, 122, 432  
 Reipurth, B., Bally, J., Devine, D. 1997a, *AJ*, 114, 2708  
 Reipurth, B., Hartigan, P., Heathcote, S. et al. 1997b, *AJ*, 114, 757  
 Reipurth, B., Bally, J., Fesen, R.A., Devine, D. 1998, *Nature*, 396, 343  
 Reipurth, B., Armond, T., Raga, A.C., Bally, J. 2003, *ApJ*, 593, L47  
 Reipurth, B., Mikkola, S., Connelley, M., Valtonen, M. 2010, *ApJ*, 725, L56  
 Reipurth, B., Clarke, C.J., Boss, A.P. et al. 2014, *Protostars and Planets VI*, eds. H. Beuther et al., University of Arizona Press, p. 267  
 Sahan, M. & Haffner, L.M. 2016, *AJ*, 151:A147  
 Sharpless, S., 1959, *ApJS*, 4, 257  
 Smith, N., Bally, J., Walborn, N.R. 2010, *MNRAS*, 405, 1153  
 Sterzik, M.F. & Durisen, R.H. 1998, *A&A*, 339, 95

- Sugitani, K., Fukui, Y., Ogura, K. 1991, *ApJS*, 77, 59  
Takami, M., Karr, J.J., Koh, H. et al. 2010, *ApJ*, 720, 155  
Terebey, S., Vogel, S.N., Myers, P.C. 1992, *ApJ*, 390, 181  
Tofflemire, B., Mathieu, R.D., Ardila, D.R. et al. 2017, *ApJ*, 835:A8  
Valtonen, M. & Mikkola, S. 1991, *Ann. Rev. Astron. Astrophys.*, 29, 9  
Wade, C.M. 1957, *AJ*, 62, 148  
Zhang, C.Y., Laureijs, R.J., Chlewicki, G., 1989, *A&A*, 218, 231  
Zucker, C., Speagle, J.S., Schafly, E.F. et al. 2019, *ApJ*, 879, 125  
Zucker, C., Speagle, J.S., Schafly, E.F. et al. 2020, *A&A*, 633, A51

**Table A1.** Flux Values for IRAS 05417+0907

$\lambda$ [ $\mu\text{m}$ ]	$\nu F_\nu$ [ $\text{Wm}^{-2}$ ]	Source
1.24	$1.60 \cdot 10^{-16}$	2MASS J
1.65	$1.82 \cdot 10^{-15}$	2MASS H
2.16	$3.33 \cdot 10^{-15}$	2MASS K
3.35	$1.64 \cdot 10^{-14}$	WISE W1
3.55	$3.77 \cdot 10^{-14}$	IRAC1
4.49	$6.74 \cdot 10^{-14}$	IRAC2
4.60	$5.72 \cdot 10^{-14}$	WISE W2
5.73	$8.16 \cdot 10^{-14}$	IRAC3
7.87	$7.81 \cdot 10^{-14}$	IRAC4
11.6	$3.86 \cdot 10^{-14}$	WISE W3
11.6	$6.39 \cdot 10^{-14}$	IRAS
18.4	$1.51 \cdot 10^{-13}$	AKARI
22.1	$2.21 \cdot 10^{-13}$	WISE W4
23.7	$1.47 \cdot 10^{-13}$	MIPS
23.9	$3.49 \cdot 10^{-13}$	IRAS
61.8	$1.21 \cdot 10^{-12}$	IRAS
65.0	$1.10 \cdot 10^{-12}$	AKARI
71.4	$6.13 \cdot 10^{-13}$	MIPS
102	$2.20 \cdot 10^{-12}$	IRAS
160	$1.36 \cdot 10^{-12}$	AKARI
447	$5.36 \cdot 10^{-14}$	SCUBA2
855	$4.45 \cdot 10^{-15}$	SCUBA2

**APPENDIX A: ENERGY DISTRIBUTION**

The following table lists the fluxes for the photometric measurements shown in Figure 5.